

# Superparamagnetic response of Fe-coated W tips in spin-polarized scanning tunneling microscopy

Soo-hyon Phark,<sup>1</sup> Jeison A. Fischer,<sup>1,2</sup> Marco Corbetta,<sup>1</sup> Dirk Sander,<sup>1,\*</sup> and Jürgen Kirschner<sup>1,3</sup>

<sup>1</sup>*Max-Planck-Institut für Mikrostrukturphysik,  
Weinberg 2, 06120 Halle, Germany*

<sup>2</sup>*Laboratório de Filmes Finos e Superfícies, Departamento de Física,  
Universidade Federal de Santa Catarina, Florianópolis, SC, Brazil*

<sup>3</sup>*Institut für Physik, Martin-Luther-Universität Halle-Wittenberg, 06120 Halle, Germany*

(Dated: March 19, 2019)

## Abstract

We performed spin-polarized scanning tunneling spectroscopy on biatomic-layer-high Co nanoislands grown on Cu(111) in magnetic fields oriented normal to the sample surface, with Fe-coated W tips. Increasing the temperature from 10 to 30 K, we observe a reduced slope of the differential conductance around zero field. A quantitative analysis of the field- and temperature-dependent differential conductance data in the framework of superparamagnetism as described by a Langevin function gives an excellent description of the experimental results. The analysis suggests that a Fe nano-apex at the W tip, which is composed of 220–300 Fe atoms, determines the magnetic response of the tip.

PACS numbers: 68.37.Ef, 75.60.Ej, 75.20.En, 75.75.-c

Spin-polarized scanning tunneling microscopy/spectroscopy (SP-STM/S)<sup>1-3</sup> has been successfully applied to characterize spin-ordering,<sup>4,5</sup> spin-dependent electron confinement,<sup>6</sup> and magnetization reversal<sup>7-9</sup> of individual nanostructures. The method relies on the dependence of the tunnel current and the differential conductance on the relative magnetization orientation between tip and sample. However, in spite of its pivotal function in SP-STM, quantitative insights regarding the magnetization state of the tip are scarce.<sup>10,11</sup>

In a previous study we have characterized the magnetic response of tips by in-field SP-STM measurements.<sup>10</sup> Tips used in SP-STM can be classified in three categories with respect to their response to an external magnetic field: 1) the tip magnetization orientation is fixed and unaffected by the external magnetic field, 2) the tip magnetization orientation is bistable and switches by the external magnetic field, and 3) the tip magnetization direction follows the external magnetic field. The identification of the magnetic tip response from field-dependent measurements of the differential conductance has been described before.<sup>10</sup> Here we focus on case 3), where we exploit the temperature dependence of SP-STS measurements in magnetic fields to characterize the magnetization state of the tip quantitatively.

To this end we measure the magnetic field and temperature dependence of the differential conductance on biatomic-layer-high (BLH) Co nanostructures on Cu(111) with a prototypical tip used in SP-STM, a Fe-coated W tip. We observe a considerable decrease of the slope of the differential conductance  $dI/dV(H)$  around zero field with increasing temperature from 10 to 30 K. Our quantitative analysis reveals that this behavior can be ascribed to a superparamagnetic response of the tip with a magnetic moment of  $660 \pm 10 \mu_B$ . We attribute the magnetic response of the tip to a Fe nano-apex with approximately 220–300 atoms.

The experiments were performed in an ultra-high vacuum (UHV) chamber (base pressure  $< 1 \times 10^{-11}$  mbar) equipped with a scanning tunneling microscope operating at 10 K. The sample temperature was measured in close proximity of the sample plate in the STM head. In order to obtain a magnetic contrast, we deposited 40 monolayers Fe on an electrochemically etched W tip, which was briefly heated in UHV up to 2400 K for 2 sec, as checked

by a pyrometer, prior to Fe deposition. Then the Fe-coated W tip was annealed at a lower temperature of less than 1000 K for 5 sec. The Cu(111) single crystalline substrate was cleaned by repetitions of Ar<sup>+</sup>-sputtering (1 keV, 0.75  $\mu$ A sample current, 15 min per cycle) and subsequent heating at 700 K for 15 minutes until defect-free, atomically flat, and large ( $\gtrsim$  200 nm) terraces are observed in STM. We deposited 0.24 monolayer Co, then subsequently, 0.28 monolayer Fe on the cleaned Cu surface at room temperature in UHV. This sequential deposition of two materials produced two different types of islands on the Cu substrate, Fe-decorated Co island and isolated Fe island, where coverage and island composition are checked in situ by STM. STM and STS on a Fe-decorated Co island revealed that the distinction between Co and Fe is possible by a difference in apparent heights and pronounced differences in the differential conductance.<sup>13,14</sup> We employed a lock-in technique with a modulation bias voltage  $V_b$  at a frequency  $\nu = 4$  kHz and root-mean square amplitude of 20 mV to detect  $I(V)$  and  $dI/dV$  simultaneously.

Figure 1(a) shows a constant-current STM (CC-STM) topographic image of typical Fe-decorated Co islands. The inner region of the islands are enclosed by dotted lines and labeled by ‘1’ and ‘2’, and they identify the Co cores, as checked by spatial resolved STS. A line profile across the island distinguishes three regions of the island, as shown in the inset. The Co core is surrounded by a Fe rim with two different structural phases ‘Fe-a’ and ‘Fe-b’, which were discussed earlier as fcc- and bcc-stacking BLH Fe on Cu(111),<sup>13,14</sup> respectively. Figure 1(b) shows the STS spectra measured on the Cu(111) surface and at the centers of the Co cores 1 and 2, as marked by the crosses in Fig. 1(a). The STS spectra on the Cu region and at the center of each Co core show the onset of the surface state of Cu(111)<sup>15</sup> and the sharp  $3d_{z^2}$ -like surface states of Co<sup>16</sup> at the bias voltages of  $V_b = -0.4$  V and  $-0.3$  V, as indicated by the black and green vertical bars, respectively.

Figures 2(a) and (b) show the STS spectra of Co cores 1 and 2, respectively, measured at a sample temperature of 10 K. The spectra show clear field-dependent changes. We measured the differential conductance spectra with the external field swept between  $-2.5$  and  $+2.5$  T along the sample normal. Thus we obtain field-dependent differential conductance  $dI/dV$

data. We identify a bias voltage  $V_b$  which gives a clear field-dependent change of the signal, and we choose  $-0.87$  V here. Figures 2(c) and (d) show the differential conductance  $dI/dV(H)$  hysteresis loops extracted from the  $dI/dV$  values at  $V_b = -0.87$  V at three temperatures 10, 20, and 30 K for Co cores 1 and 2, respectively. The data have been obtained with the same tip.

The hysteresis loops in Figs. 2(c) and (d) show symmetric butterfly-shaped curves. This identifies a tip response according to the class 3) scenario as defined above, where the tip magnetization follows the external field. The sudden drop of the signal at 1.6 T (2.0 T) for Co core 1 (2) indicates the switching of the magnetization direction of the Co core.<sup>9</sup> A gradual change of the differential conductance signal in the field range below the switching field  $H_{sw}$  is observed for both Co cores. Note that the switching field is reduced from 1.55 to 1.05 T (from 1.95 to 0.85 T) for Co core 1 (2) as the temperature increases from 10 to 30 K. This implies that the magnetization reversal processes of the Co cores can be ascribed to thermally assisted magnetization reversal.<sup>9,17,18</sup>

Here, we focus on the magnetic response of the tip to the external magnetic field at different temperatures. The curves of Figs. 2(c) and (d) indicate that the slope of the differential conductance around 0 T gets smaller with increasing temperature. In this field and temperature range we can assume a constant magnetization of the Co cores, thus we ascribe the observed changes of the differential conductance signal to the tip response to the field and temperature. The individual data points show a saturation of the signal with increasing magnitude of the field, and the saturation field increases with increasing temperature. This behavior suggests a superparamagnetic response of the tip.

To support and quantify this assertion, we analyze the differential conductance signal in the field range below the switching field of Co, as shown in Figs. 3(a) and (b), for Co cores 1 and 2, respectively. We fit the individual differential conductance data points in the framework of superparamagnetism<sup>12</sup> by a Langevin function

$$\frac{dI}{dV}(H) = \left(\frac{dI}{dV}\right)_{sat} \left[ \coth \frac{m_{tip}\mu_0(H - H_{off})}{k_B T} - \frac{k_B T}{m_{tip}\mu_0(H - H_{off})} \right] - \left(\frac{dI}{dV}\right)_C. \quad (1)$$

We introduce the saturation of the differential conductance  $(dI/dV)_{sat}$  and the differential conductance offset  $(dI/dV)_C$ , which determines the average of the two differential conductance saturations for the parallel and antiparallel configurations between tip and sample magnetization. We also introduce the offset field  $H_{off}$ , to consider the magnetic-stray-field-induced shift of the curves by  $\sim 60$  mT to the positive field direction for a field sweep from negative to positive values. This stray field originates from the magnetization of the Co core pointing into the negative field direction. The differential conductance data are normalized to a saturation value of  $\pm 1$ . The solid curves through the data points of Figs. 3(a) and (b) are fits using the equation (1), and they describe the data very well. The fitting procedure gives a total magnetic moment  $m_{tip}$  of around  $660 \pm 30 \mu_B$  for all measurements.

The convincing description of the experimental data by the Langevin approach strongly implies a superparamagnetic response of the tip. This assessment is further corroborated by plotting all data points as a function of  $\mu_0 H/T$ , and the condensation of all data on a single curve, as shown in Fig. 3(c), is the hallmark of a superparamagnetic response.<sup>12</sup> We extract a total magnetic moment of  $660 \pm 10 \mu_B$  from the Langevin fit of the data. In a first approximation, we ascribe this total magnetic moment to a macrospin, where all individual spins respond in unison to the external field. Based on a previous experimental study of the magnetic moment of Fe nanoclusters,<sup>19</sup> we may assume a magnetic moment of  $2.2\text{--}3 \mu_B$  per single Fe atom. This leads us to speculate that a nano-apex of approximately  $220\text{--}300$  Fe atoms determines the magnetic response of the tip.

We use the superparamagnetic criterion,  $25k_B T \geq K_a V$ ,<sup>12</sup> to estimate the upper limit for the magnetic anisotropy as  $K_a \leq 0.07\text{--}0.1$  meV/atom for  $300\text{--}220$  Fe atoms, respectively. Thus, even a considerably increased magnetic anisotropy per Fe atom of the nano-apex as compared to bulk Fe ( $\sim 0.0035$  meV/atom)<sup>20</sup> would still fulfill the superparamagnetic criterion. In spite of the convincing description of our data with a macrospin model, we can not exclude a more complicated arrangement of the magnetic structure at the nano-apex which also results in the same total magnetic moment of  $660 \mu_B$ .

We analyzed seven Fe-coated W tips, which were prepared under the same conditions

as described above. In all cases we found a very good description of the experimental data by a superparamagnetic response. The analysis revealed a total magnetic moment between 100 and 2000  $\mu_B$ . This finding suggests that the same macroscopic tip preparation by Fe deposition and annealing may lead to different nano-apices with 30–900 Fe atoms, which determine the magnetic response of the tip.

The field-dependences of the magnetic responses of tips in this study can be characterized by two main aspects: (a) non-hysteretic behavior and (b) smooth S-shape change at a magnetic field  $\mu_0 H < \mu_0 H_{Co}$ . Although there is not a complete structural characterization of a Fe-coated W tip apex yet, previous field ion microscopy (FIM) studies on W tips indicate a W(110) face at the apex with a lateral extension of a few nm.<sup>21,22</sup> Thus, to discuss the magnetic anisotropy it appears to be proper as a first approach to refer to the well studied system Fe/W(110). Both Fe films<sup>23,24</sup> and nanoislands<sup>25,26</sup> grown on W(110) have shown an in-plane magnetic anisotropy. Thus one could be inclined towards another picture of the magnetic response, namely a magnetic field induced rotation of the tip magnetization from parallel to perpendicular to the sample plane with increasing magnetic field. However, the resulting effect of the temperature change on the field-dependence of tip magnetization suggests a decreasing saturation field with increasing temperature, in contrast with our observation, and we disregard this model here.

The atomic processes leading to the formation of a nano-apex are currently not directly accessible experimentally. But the resulting nano-apex is magnetically characterized, as demonstrated here, and this is mandatory for a reliable interpretation of SP-STM/S data. To appreciate the origin of nano-apices in a STM tip we recall that double tip effects are a common observation in STM images.<sup>27,28</sup> This means that protrusions at the tip apex with nm extensions are readily formed, and they determine the tunneling characteristics. We speculate that the high electric field of an order of V/nm between tip and sample and the morphology of the Fe-coverage at the W tip are factors contributing to nano-apex formation.

In conclusion, we characterized the magnetic response of Fe-coated W tips by in-field SP-STs measurements at different temperatures. We find that the temperature-dependent

magnetic hysteresis of the differential conductance can be ascribed to a superparamagnetic response of a Fe nano-apex at the tip, which determines the spin-dependent tunneling properties.

This work was partially supported by Deutsche Forschungsgemeinschaft grant SFB 762. We thank N. Kurowsky for expert technical support.

---

\* Electronic address: sander@mpi-halle.mpg.de

- <sup>1</sup> W. Wulfhekel and J. Kirschner, *Appl. Phys. Lett.* 75, 1944 (1999).
- <sup>2</sup> M. Bode, *Rep. Prog. Phys.* 66, 523 (2003).
- <sup>3</sup> S. Rusponi, N. Weiss, T. Cren, M. Epple, and H. Brune, *Appl. Phys. Lett.* 87, 162514 (2005).
- <sup>4</sup> C. L. Gao, W. Wulfhekel, and J. Kirschner, *Phys. Rev. Lett.* 101, 267205 (2008).
- <sup>5</sup> R. Wiesendanger, *Rev. Mod. Phys.* 81, 1495 (2009).
- <sup>6</sup> H. Oka, P. A. Ignatiev, S. Wedekind, G. Rodary, L. Niebergall, V. S. Stepanyuk, D. Sander, and J. Kirschner, *Science* 327, 843 (2010).
- <sup>7</sup> O. Pietzsch, A. Kubetzka, M. Bode, and R. Wiesendanger, *Phys. Rev. Lett.* 92, 057202 (2004).
- <sup>8</sup> G. Rodary, S. Wedekind, D. Sander, and J. Kirschner, *Jpn. J. Appl. Phys.* 47, 9013 (2008).
- <sup>9</sup> S. Ouazi, S. Wedekind, G. Rodary, H. Oka, D. Sander, and J. Kirschner, *Phys. Rev. Lett.* 108, 107206 (2012).
- <sup>10</sup> G. Rodary, S. Wedekind, H. Oka, D. Sander, and J. Kirschner, *Appl. Phys. Lett.* 95, 152513 (2009).
- <sup>11</sup> M. Corbetta, S. Ouazi, J. Borme, Y. Nahas, F. Donati, H. Oka, S. Wedekind, D. Sander, and J. Kirschner, *Jap. J. Appl. Phys.* 51, 030208 (2012).
- <sup>12</sup> C. P. Bean and J. D. Livingston, *J. Appl. Phys.* 30, S120 (1959).
- <sup>13</sup> A. Biedermann, W. Rupp, M. Schmid, and P. Varga, *Phys. Rev. B* 73, 165418 (2006).
- <sup>14</sup> L. Gerhard, T. K. Yamada, T. Balashov, A. F. Takacs, R. J. H. Wesselink, M. Dane, M. Fechner, S. Ostanin, A. Ernst, I. Mertig, and W. Wulfhekel, *Nature Nanotech.* 5, 792 (2010).
- <sup>15</sup> M. F. Crommie, C. P. Lutz, and D. M. Eigler, *Nature(London)* 363, 524 (1993).
- <sup>16</sup> L. Diekhöner, M. A. Schneider, A. N. Baranov, V. S. Stepanyuk, P. Bruno, and K. Kern, *Phys. Rev. Lett.* 90, 236801 (2003).

- <sup>17</sup> L. Néel, J. Phys. Rad. 2, 49 (1950).
- <sup>18</sup> W. F. Brown, Phys. Rev. 130, 1677 (1963).
- <sup>19</sup> I. M. L. Billas, J. A. Becker, A. Chârelain, and W. A. de Heer, Phys. Rev. Lett. 71, 4067 (1993).
- <sup>20</sup> M. B. Stearns 1986 *Magnetic Properties of 3d, 4d, and 5d Elements Alloys and Compounds* (Landolt-Bornstein Numerical Data and Functional Relationships in Science and Technology Group III, vol 19a) (Berlin: Springer).
- <sup>21</sup> J. A. Panitz, J. Phys. E: Sci. Instrum. 15, 1281 (1982).
- <sup>22</sup> R. Gomer 1961 *Field Emission and Field Ionization*. Number 9 in Harvard Monographs in Applied Science (Harvard University Press).
- <sup>23</sup> H. J. Elmers and U. Gradmann, Appl. Phys. A 51, 255 (1990).
- <sup>24</sup> H. J. Elmers, J. Hauschild, and U. Gradmann. Phys. Rev. B 54, 15224 (1996).
- <sup>25</sup> M. Bode, A. Wachowiak, J. Wiebe, A. Kubetzka, M. Morgenstern, and R. Wiesendanger, Appl. Phys. Lett. 84, 948 (2004).
- <sup>26</sup> S. Krause, L. Berbil-Bautista, G. Herzog, M. Bode, and R. Wiesendanger, Science 317, 1537 (2007).
- <sup>27</sup> S. -I. Park, J. Nogami, and C. F. Quate, Phys. Rev. B 36, 2863 (1987).
- <sup>28</sup> J. P. Pelz and R. H. Koch, Phys. Rev. B 41, 1212 (1990).

## Figures

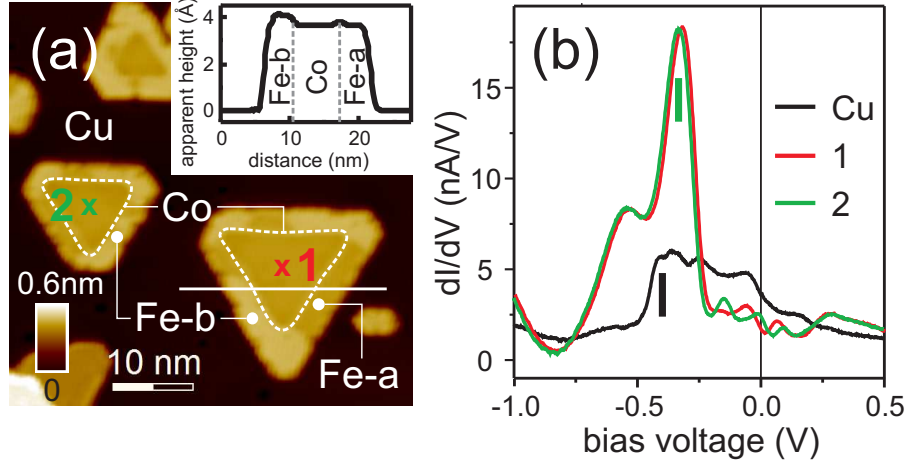


FIG. 1: (Color online) (a) Constant-current STM image of two triangular Co cores of Fe-decorated Co islands on which the magnetic-field-dependent  $dI/dV$  are measured. The inset shows the apparent constant-current STM height profile along the white solid line. (b) shows the STS spectra measured on the Cu(111) surface and at the centers of Co cores ‘1’ and ‘2’ in (a). The STM image in (a) is measured with  $V_b = 0.2$  V and  $I_{set} = 1$  nA. STS spectra in (b) are measured with  $V_{stab} = 0.5$  V and  $I_{stab} = 1$  nA.

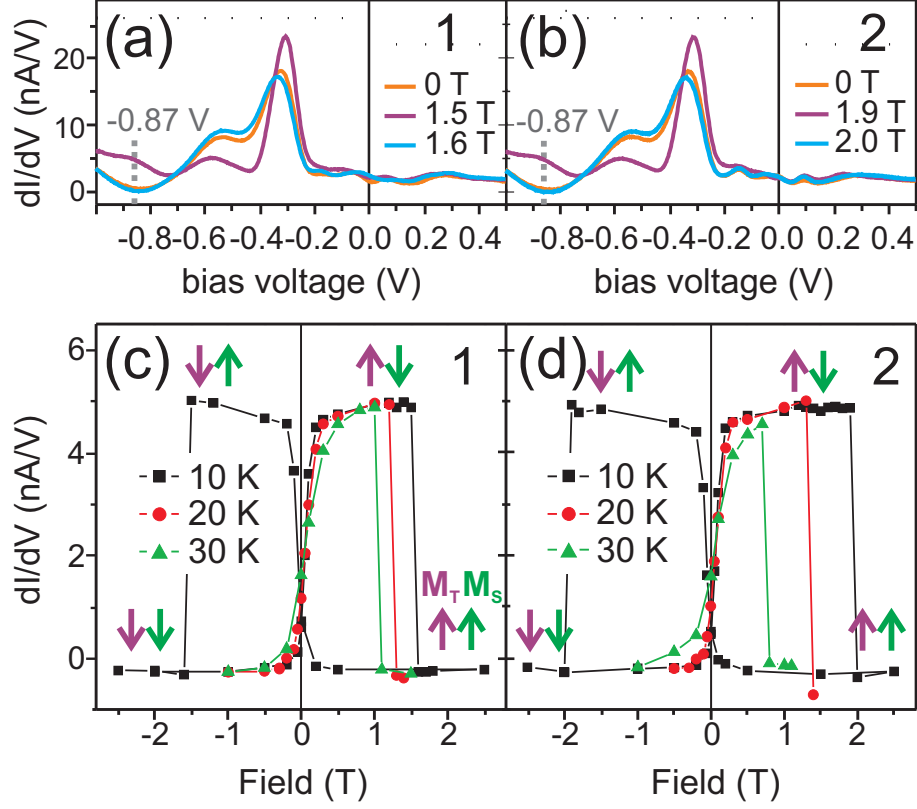


FIG. 2: (Color online) STS spectra measured at the centers of Co cores (a) ‘1’ and (b) ‘2’ identified in Fig. 1(a), in external magnetic fields perpendicular to the sample surface. The field values 1.5 and 1.6 T (1.9 and 2.0 T) in (a) ((b)) correspond to the magnetic fields below and above the magnetization reversal of the Co core ‘1’ (‘2’), respectively. Hysteresis loops of the differential conductance  $dI/dV$  (at  $V_b = -0.87$  V) at 10, 20, and 30 K measured at the center of Co cores ‘1’ (c) and ‘2’ (d). All STS spectra are measured with an open feedback loop at stabilization parameters  $V_{stab} = 0.5$  V and  $I_{stab} = 1$  nA.

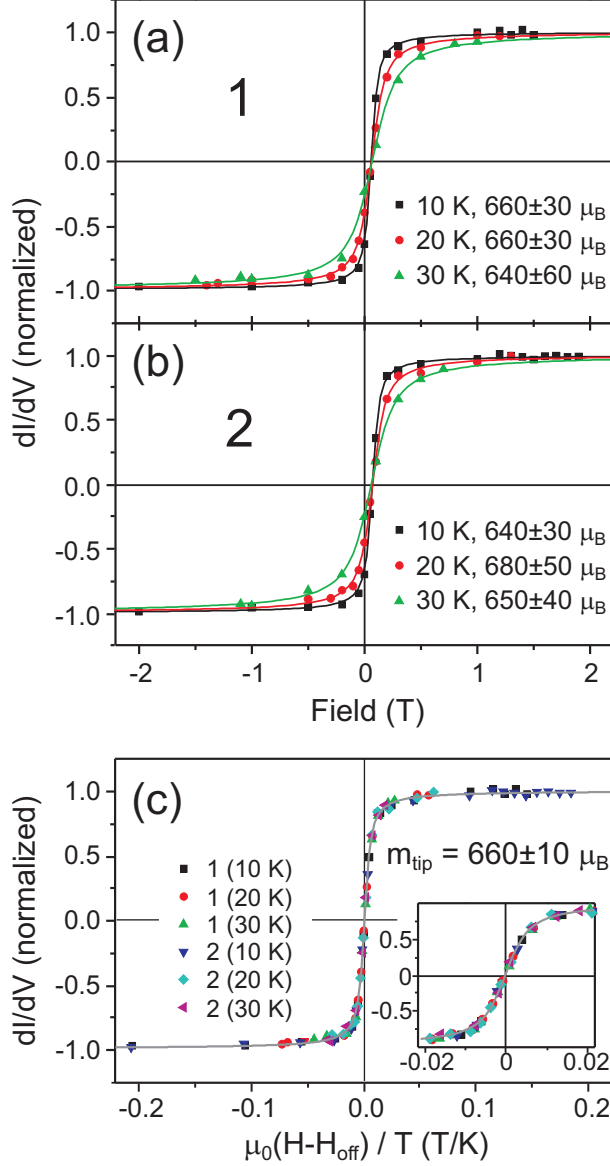


FIG. 3: (Color online) Magnetic-field-dependent differential conductance  $dI/dV$  plots in (a) and (b) extracted from the hysteresis loops of Figs. 2(c) and (d), respectively. The differential conductance  $dI/dV$  curves at each temperature are normalized by fitting with equation (1), as shown by the solid curves. The legend gives the measurement temperature and the total magnetic moment in  $\mu_B$ , as extracted from the fit of the data with the equation (1). (c) Plots of all  $dI/dV$  values as a function of reduced magnetic field ( $\mu_0 H/T$ ). The inset is a close-up of the plots around  $\mu_0(H-H_{off})/T = 0$ . The gray curve shows the Langevin fit in one curve for all data.